

# Smart Manufacturing and Material Processing (SMMP)

DOI: http://doi.org/10.26480/smmp.01.2023.54.58



#### RESEARCH ARTICLE



# EFFECT OF LOW TEMPERATURE AND LOW SPEED DIFFERENTIAL TEMPERATURE EXTRUSION ON THE PERFORMANCE OF MG-6AL-1ZN-0.15MN ALLOY

Zibo Meng<sup>a</sup>, He Ma<sup>b</sup>, Fanzhi Meng<sup>a,\*</sup>, Qiang Yang<sup>c</sup>, Xin Qiu<sup>c</sup>, R.P. Sihombing<sup>d</sup>

- <sup>a</sup>School of Materials Science and Engineering, Changchun University of Science and Technology, Changchun, Jilin, China
- bSchool of Materials Science and Engineering, Jilin University, Changchun, Jilin, China
- State Key Laboratory of Rare Earth Resource Utilization, Changchun Institute of Applied Chemistry, Changchun, Jilin, China
- <sup>d</sup>Department of Chemical Engineering, Politeknik Negeri Bandung, Bandung, Indonesia
- \*Corresponding Author Email: fzmeng@cust.edu.cn

This is an open access article distributed under the Creative Commons Attribution License CC BY 4.0, which permits unrestricted use, distribution, and reproduction in any medium, provided the original work is properly cited.

### **ARTICLE DETAILS**

#### Article History:

Received 20 January 2024 Revised 18 February 2024 Accepted 11 March 2024 Available online 15 March 2024

### **ABSTRACT**

Magnesium alloys with the hexagonal close-packed crystal structure have the low formability and weaker mechanical properties, contracted with Ti and Al alloys, which also limits the application in aerospace, aviation and automobile fields. Therefore, it is a big deal to invest the effect of low temperature and low speed differential temperature extrusion (DTE) on the microstructure and mechanical properties of mg-6al-1zn-0.15 MN (AZ61) alloy. In this work ,The AZ61 alloy was prepared by differential temperature extrusion (the ingoting temperature is 450 °C, the mould temperature is 90 °C, the extrusion ratio is 7:1) with finer recrystallized grains (DRX) ,obvious < 01-10 > texture, non-recrystallized grains with high density of dislocations. At last, this work indicates that AZ61 alloy used DTE technology to equip with bimodal grain structure, the grains in the non-recrystallization region provide high-density dislocations, and the grains in the recrystallization region provide grain boundary strengthening. Which is the origin of the mechanical properties improved greatly.

# KEYWORDS

Severe plastic deformation (SPD); differential temperature extrusion (DTE); AZ61; double-peak structure; mechanical property

# 1. Introduction

Currently, the Mg-6Al-1Zn-0.15Mn (AZ61) alloy is a widely used, low-cost commercial magnesium alloy. It is known for its low density, high specific strength and stiffness, excellent machinability, and high recyclability, making it a "green energy material" compared to steel and aluminum alloys. As companies increasingly focus on improving energy efficiency, reducing energy consumption by reducing vehicle weight has become a priority. Magnesium alloys have gained attention due to their low density. However, the limited structural application of magnesium alloys is attributed to their weak mechanical properties. But adding rare-earth elements has raised costs. MG alloy has a strong grain boundary strengthening response. Ultra-fine grain structure (grain size < 1  $\mu$ m) is a common method to obtain super-strength MG alloys, SPD is an effective method to prepare ultrafine grains (Wang et al., 2021). Therefore, the ultra-fine grain AZ61 magnesium alloy was prepared by SPD method.

Studies have shown that commercial magnesium alloys are processed by severe plastic deformation to achieve the purpose of grain refinement, so as to improve the strength of magnesium alloys. M.T. et al. achieved a UTS of 405 MPa in AZ91 through accumulative roll bonding (ARB), H. Miura et al. improved the tensile yield strength of AZ61 to 480 MPa using multidirectional forging (MDF), buts with a limited elongation of 5% (Perez-Prado et al., 2005; Miura et al., 2012). B.Q. Shi et al. enhanced the TYS of AZ80 to 347 MPa and UTS to 434 MPa using equal-channel angular pressing (ECAP) (Shia et al., 2012). W.J. Kim et al. processed AZ91 using high-ratio differential speed rolling (HRDSR) and achieved a TYS of 410 MPa and a UTS of 467 MPa after aging treatment at 373 K (Kim et al., 2009).

However, these processes are difficult to commercialize due to continuous processing and material size limitations. Additionally, Sasaki achieved obvious improvements in the mechanical properties of Mg-9.8Sn-1.2Zn-1.0Al alloy, with a TYS of 308 MPa, UTS of 354 MPa, and elongation of 12%, by employing a combination of low-temperature (250°C) and slow-speed extrusion (0.1 mm/s). The low temperature and slow-speed combination promoted the formation of a large quantity of dynamic precipitates, inhibiting the growth of recrystallized grains and thus enhancing the alloy's strength (Sasaki et al., 2008).

This study attempts to utilize differential temperature extrusion (DTE) to prepare high-strength Mg-6Al-1Zn-0.15Mn (AZ61) alloy through grain refinement under low temperature and slow-speed (0.1mm/s) conditions. The potential mechanisms underlying the improvement of strength characteristics will be analyzed from a microscopic structural perspective.

# 2. EXPERIMENTAL PROCEDURE

# 2.1 Preparation of Samples

The effects of carbon dioxide and 0.8 vol. As-cast AZ61 alloy was obtained by melting in SF6 atmosphere. Cylindrical ingots 100mm long and 95mm in diameter were obtained by cutting. The ingot was homogenized at 420 °C for 16 hours. The ingot with 100mm length and 85mm diameter can be turned by turning the homogenized ingot. Raise the temperature of the extruder and die (32 mm in diameter) to 90 °C, The ingot was kept at 450 °C for 2 hours, Then extrude (at a speed of 0.1 mm/min), The AZ61 extruded bar (Az61-450-90) was obtained by low temperature, low speed and low extrusion ratio DTE (extrusion ratio is 7:1)

Quick Response Code Access this article online



Website:

**DOI:** 10.26480/smmp.01.2023.54.58

Website: www.topicsonchemeng.org.my

#### 2.2 Microstructures

The characterization observations used an optical microscope (OM, Olympus-GX71), a scanning electron microscope (SEM, Hitachi S-4800, equipped with an EDS spectrometer) (accelerating voltage of 10kv, current of  $10\mu A)$ , and electron backscatter diffraction (EBSD, Qunta250), and TEM (transmission electron microscopy, FEI Tecnai  $G^2$  F20). The samples were ground with silicon carbide sandpaper of different roughness and polished to a smooth surface without obvious scratches. The etchant used was a 4% Dilute nitric acid cerium solution for OM and SEM observation and characterization, and elemental quantitative analysis using an EDS spectrometer (accelerating voltage of 20kv, current of  $15\mu A$ ). The sample for electron backscatter diffraction (EBSD) needs to be electropolished

with  $AC_2$  solution at -20°C for about 50s after polishing. EBSD collected data with a step size of 0.8 $\mu$ m, and then used HKL Channel 5 software to analyze the degree of recrystallization, grain size, Schmid factor, average grain orientation difference, dislocation density, and texture strength.

#### 2.3 Mechanical Properties

The extruded rod is processed into a dog-bone-shaped tensile rod (gauge length of 36mm, specification diameter of 6mm) and stretched at a speed of 2.160mm/min. The cylindrical compression rod (gauge length of 12mm, specification diameter of 6mm) is compressed at a speed of 0.720mm/min. The experiment was carried out at room temperature using a CRIMS-DDL100 electronic universal testing machine.

# 3. RESULT AND DISCUSSION

#### 3.1 Mechanical Properties

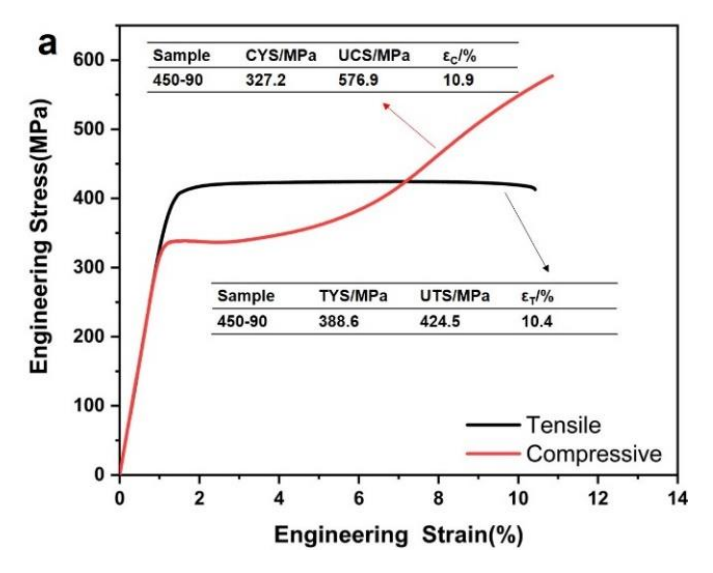


Figure 1: Engineering stress-strain curve, tensile curve

The stress-strain curve and mechanical properties of AZ61 alloy after the DTE process are depicted in Figure 1. The tensile performance is represented by the black solid line, which includes a tensile yield strength (TYS) of 388.6MPa, an ultimate tensile strength (UTS) of 424.5MPa, and a fracture elongation ( $\epsilon_T$ ) of 10.4%. The red solid line signifies the compressive performance, encompassing a compressive yield strength (CYS) of 327.2MPa, an ultimate compressive strength (UCS) of 576.9MPa, and a fracture elongation ( $\epsilon_C$ ) of 10.9%. The AZ61 alloy also exhibits yield asymmetry (CYS/TYS=0.84). The contributions of solid solution strengthening, dislocation strengthening, grain boundary strengthening, second phase strengthening, and texture strength to the yield strength are obvious. The tensile strength (YS) of extruded alloys can be estimated using the formula:  $\sigma_Y = \sigma_0 + \Delta \sigma_{gs} + \Delta \sigma_{crowan} + \Delta \sigma_p$ , where  $\sigma_0$  denotes the intrinsic lattice resistance of Mg against basal slip, with a value of 11 MPa (Cheng et al., 2014).

# 3.2 Mechanism of Strengthening

The contribution of solid solution strengthening to strength can be calculated using the model proposed by Gypen and Deryutere (Cheng et al., 2014).

$$\Delta\sigma = \left(\sum_{i} k_{i}^{\frac{1}{n}} C_{i}\right)^{n} \tag{1}$$

Here n is a constant with a value of 2/3 (Cheng et al., 2014).  $k_i$  represents the strengthening constant of the solute i, and  $C_i$  denotes the concentration of solute i. In this study, the concentrations of Zn and Mn are low, and the AlMn phase was precipitated. Hence, the calculations here focus only on the strength Al provides to the alloy in solid solution strengthening, as indicated by the formula:

$$\Delta\sigma = \left(K_{Al}^{\frac{1}{n}}C_{Al}\right)^n\tag{2}$$

 $k_{\rm Al}$  is 196MPa (at. %)-²/³**Error! Reference source not found.**,  $C_{\rm Al}$  is the concentration of Al, and it is equal to 3at. %. The solid solution strengthening value for the AZ61 alloy is approximately 18.9 MPa, as determined by calculations.

Figure 2 depicts the microstructural characteristics of AZ61 alloy following the DTE-450-90 treatment. The SEM images, taken parallel to the extrusion direction (ED), reveal that a obvious reduction in grain population occurs after the extrusion process, numerous small dynamic precipitation phases are formed and distributed along the direction of extrusion. Moreover, block-shaped secondary phases were observed, and their chemical composition within the red dashed boxes in the SEM images was determined to be AlMn using energy-dispersive X-ray spectrometry (eds).

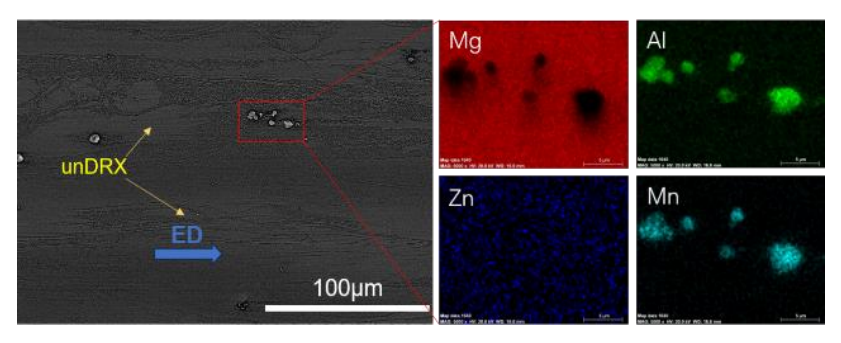


Figure 2: The SEM of AZ61 after DTE-450-90 and eds image and eds of A blocky second phase

Figure 3: A is Bright-field TEM (BF-TEM) images of a recrystallized region; b is Electron diffraction pattern

As shown in the Figure 3 abundant  $Mg_{17}Al_{12}$  precipitates along the grain boundaries in the recrystallization region are evident from the bright field and high-resolution images obtained through transmission electron microscopy. In this study, spherical  $Mg_{17}Al_{12}$  is identified as the primary dynamic precipitation phase, and it is characterized by a very low Mn content. c Thus, the formulation of Orowan's equation for spherical second phase strengthening is (Cheng et al., 2014):

$$\Delta \sigma Orowan = \frac{MGb}{2\pi\sqrt{1-\nu}} \frac{1}{\lambda} ln \frac{d_P}{r_0}$$
 (3)

Here M represents the Taylor factor (with a value of 3.6), G is the shear modulus (for Mg it is  $1.66 \times 104$  MPa), b is the Burgers vector (for Mg it is 0.32nm), v is the Poisson's ratio (for Mg it is 0.35).  $\lambda$  is the average distance from center to center between particles (Cheng et al., 2014):

$$\lambda = (\frac{0.779}{\sqrt{f}} - 0.785) \text{ dt}$$
 (4)

 $d_p$  represents the diameter of the precipitates,  $r_0$  represents the core radius of dislocation lines, taken as |b|. Regarding ellipsoidal and spherical precipitates, it is possible to modify the Orowan equation as shown below (Zha et al., 2023).

$$\Delta \sigma Orowan = \frac{MGb}{2\pi\sqrt{1-\nu}\left(\frac{0.79}{f_t} - 0.785\right)d_t} ln \frac{0.785 d_t}{b}$$
(5)

Here f is the volume fraction of the precipitate phase, dt is the average diameter of the precipitates. Therefore, the strength contribution of the second phase is approximately 85.5 MPa.

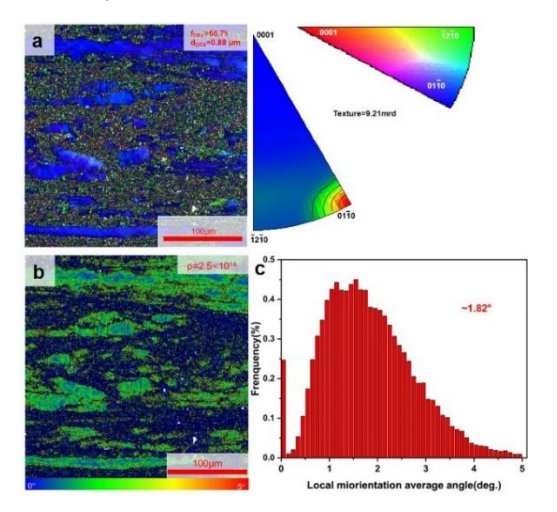


Figure 4: (a) EBSD misorientation map and inverse pole figure; (b-c) corresponding KAM map showing grains and the strain distribution.

The image in Figure 4a depicts electron backscatter diffraction (EBSD) parallel to the extrusion direction (ED). According to the statistical analysis, the volume fraction of recrystallization is measured to be 66.7%. Moreover, the recrystallized region predominantly exhibits small greencolored grains. Additionally, it incorporates fine grains in both red and purple colors, exhibiting an average grain size of 0.88 μm, which falls within the sub-micron range. In the non-recrystallized region, elongated grains exhibiting deformation are observed and they appear in a blue hue. The material showcases a clear bimodal structure, composed of both recrystallized and non-recrystallized grains. Analysis of the inverse pole figures reveals a pronounced <10-10> fiber texture in the grains deformed during extrusion, characterized by a maximum texture intensity of 9.21 mrd (maximal random disorientation). The presence of a substantial quantity of sub-micron-sized recrystallized grains in the samples of this study highlights the notable role of grain boundary strengthening. In this study, the AZ61 alloy did not undergo full recrystallization following the DTE process. Exhibits a bimodal structure. Consequently,

strengthening of grain boundaries is a combined result of both recrystallized and non-recrystallized grains (Liu et al., 2021):

$$\Delta \sigma g s = f D R X \sigma D R X + f n o n \Delta \sigma n o n \tag{6}$$

Here  $f_{DRX}$  and  $f_{non}$  denote the volume fractions of recrystallized and non-recrystallized grains, consecutively.  $\Delta\sigma_{DRX}$  and  $\Delta\sigma_{non}$  represent the individual contributions to strength by recrystallized and non-recrystallized grains, respectively.  $\Delta\sigma_{DRX}$  can be determined through the utilization of the Hall-Petch formula, as indicated by the references (Liu et al., 2021):

$$\Delta \sigma DRX = kDRXdDRX - 1/2 \tag{7}$$

Here  $k_{DRX}$  is a constant (Mg is 280 MPa  $\mu m^{-1/2}$ ).  $d_{DRX}$  is the average diameter of recrystallized grains. The estimated strength provided by the recrystallized grains is approximately 198.7 MPa. Reference provides the strength contribution of the non-recrystallized grains (Liu et al., 2021). The negligible contribution of recrystallized grains in the study samples justifies their exclusion.

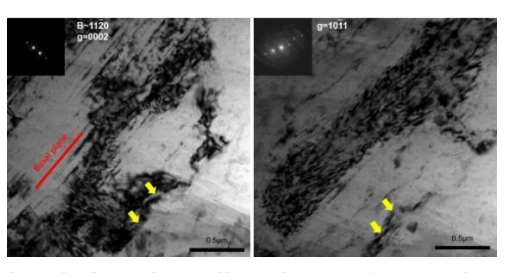


**Figure 5:** The non-recrystallized region along the [11-20] crystallographic axis of Mg was observed using bright-field transmission electron microscopy (TEM) with g=0002 and 10-11. The yellow arrows in both images mark corresponding positions.

Transmission electron microscopy (TEM) in Figure 5 was employed to observe the non-recrystallized region along the crystallographic axis, employing g=0002 and 10-11 within the same area. The subgrains contain a large number of dislocations. Through the implementation of the double-beam imaging technique, the majority of dislocations are observable at g= (0002), while they are not detectable at g= (10-11). Irrespective of their location on the basal or non-basal plane. Hence, these dislocations are classified as <a>-type dislocations. Following DTE treatment, AZ61 demonstrates a bimodal microstructure comprising non-recrystallized grains that have formed during the process of extrusion. Consequently, it exhibits a high density of geometrically necessary dislocations (GND). Taylor's formula can be used to estimate its strength contribution (Huang et al., 2015):

$$\sigma \rho = M \alpha G b \sqrt{\rho_{GND}} \tag{8}$$

Here M is the Taylor factor (with a value of 3.6),  $\alpha$  is a constant with a value

of 0.2, G is the shear modulus (with a value of 1.66×104MPa), and b is the Burgers vector (with a value of 0.32nm) (Yuan et al., 2011). The term  $\rho_{GND}$  represents the density of geometrically necessary dislocations and its estimation can be done utilizing the method outlined in reference (Yuan et al., 2011):

$$\Delta \rho \text{GND} = \frac{2\theta_{KAM}}{ab} \tag{9}$$

Here  $\theta$  is the average orientation of nuclei,  $\mu$  is the unit length (scan step size during EBSD acquisition,  $0.8\mu m$  in this study), and b is the Burgers vector (0.32nm). According to the Figure 4(b-c), the study yielded a value of  $2.5\times10^{14}m^{-2}$  for  $\Delta\rho_{GND}$ . Thus, the contribution of geometrically necessary dislocations (GND) to the strength is 60.4MPa. The calculations indicate that the AZ61 alloy achieves an overall strength of approximately 374.5MPa following DTE treatment. The obtained data from the tensile experiment exhibit consistency due to the exclusion of the strength contribution from the AlMn phase.

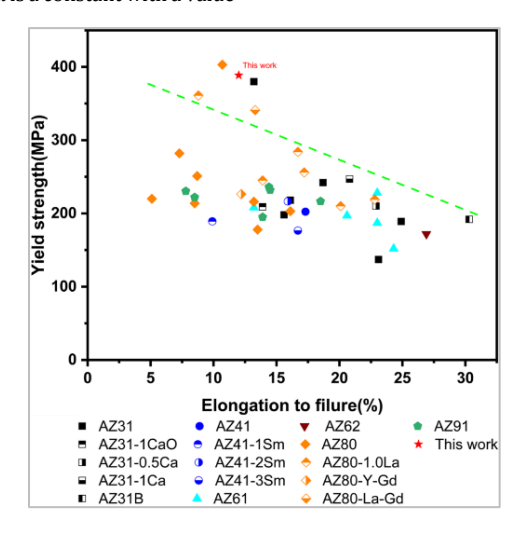


Figure 6: The strength and toughness of Azm610 are compared with other alloys in the same series. In this study, AZ31, AZ41, AZ61, AZ62, AZ80, AZ91 based on (Son et al., 2019; Liu et al., 2021; Huang et al., 2015; Bae et al., 2018; Jin et al., 2023; Yan et al., 2021)

Figure 6 presents a representative comparison in this study of the tensile engineering strength and elongation between AZ61 and other Mg-Al-Zn-Mn alloy series. The AZ61 alloy in this study demonstrates superior tensile engineering strength compared to the majority of alloys within the same series, thereby achieving a notable reduction in plastic deformation loss. The DTE process not only achieves high strength but also avoid the issues of complexity, high cost, and lack of continuity.

### 4. CONCLUSION

After differential temperature extrusion process, AZ61 samples obtained a higher strength. At the same time, the plasticity is retained to some extent:

- (1) The dominant phase that dynamically precipitates in the DTE AZ61 alloy is the fine-sized Mg<sub>17</sub>Al<sub>12</sub>. Additionally, it encompasses AlMn phases.
- (2) After DTE treatment, after undergoing DTE treatment, the microstructure of the AZ61 alloy consists of a considerable number of dynamic recrystallization areas (accounting for approximately 66.7%), Additionally, the alloy exhibits an evident <10-10> texture.
- (3) The AZ61 alloy was water-quenched after undergoing DTE treatment. Consequently, the small grain size (d = 0.88  $\mu m$ ) of the dynamic recrystallization regions increases the quantity of grain boundaries, thereby enhancing their contribution to the overall strength.
- (4) Following DTE treatment with an extrusion ratio of 7:1 incomplete recrystallization occurs in the AZ61 alloy alongside severe plastic deformation. As a result, evident deformation occurred in the non-recrystallized regions. Consequently, a substantial number of geometrically necessary dislocations are found in the non-recrystallized grains, with a density of  $2.5 \times 10^{14} \, \mathrm{m}^{-2}$ .

# REFERENCES

Bae, S.W., Kim, S.H., Lee, J.U., Jo, W.K., Hong, H.W., Kim, W., Park, S.H., 2018. Improvement of mechanical properties and reduction of yield asymmetry of extruded Mg-Al-Zn alloy through Sn addition. Journal of Alloys and Compounds, 766, Pp. 748e758.

- Cheng, W.L., Tian, Q.W., Yu, H., Zhan, H., You, H.B., 2014. Strengthening mechanisms of indirect-extruded Mg-Sn based alloys at room temperature. Journal of Magnesium and Alloys, 2, Pp. 299e304.
- Huang, X., Suzuki, K., Chino, Y., Mabuchi, M., 2015. Texture and stretch formability of AZ61 and AM60 magnesium alloy sheets processed by high-temperature rolling. Journal of Alloys and Compounds, 632, Pp. 94–102.
- Jin, S.C., Cha, J.W., Go, J., Bae, J.H., Park, S.H., 2023. Comparative study of extrudability, microstructure, and mechanical properties of AZ80 and BA53 alloys. Journal of Magnesium and Alloys, 11, Pp. 249–258.
- Kim, W.J., Jeong, H.G., and Jeong, H.T., 2009. Achieving high strength and high ductility in magnesium alloys using severe plastic deformation combined with low-temperature aging. Scripta Materialia, 61, Pp. 1040–1043.
- Liu, B.S., Wang, H.H., Zhang, Y.Z., Yang, Y.X., Ren, X.X., Du, X.Y., Hou, L.F., Wei, Y.X., Song, G.L., 2021. The influence of adding samarium on the microstructure, mechanical performance and corrosion behavior of as-extruded AZ41 alloys. Journal of Physics and Chemistry of Solids, 150, Pp. 109851.
- Liu, C., Chen, X., Chen, J., Atrens, A., Pan, F., 2021. The effects of Ca and Mn on the microstructure, texture and mechanical properties of Mg-4 Zn alloy. Journal of Magnesium and Alloys, 9, Pp. 1084–1097.
- Miura, H., Maruoka, T., Yang, X., and Jonas, J.J., 2012. Microstructure and mechanical properties of multi-directionally forged Mg–Al–Zn alloy. Scripta Materialia, 66, Pp. 49–51.
- Pérez-Prado, M.T., del Valle, J.A., Ruano, O.A., 2005. Achieving high strength in commercial Mg cast alloys through large strain rolling. Materials Letters, 59, Pp. 3299 3303.
- Sasaki, T.T., Yamamoto, K., Honma, T., Kamado, S., and Hono, K., 2008. A high-strength Mg–Sn–Zn–Al alloy extruded at low temperature. Scripta Materialia, 59, Pp. 1111–1114.

- Shia, B.Q., Chen, R.S., Ke, W., 2012. Effects of forging processing on the texture and tensile properties of ECAEed AZ80 magnesium alloy. Materials Science and Engineering A, 546, Pp. 323–327.
- Son, H.W., Lee, J.W., Hyun, S.K., 2019. Effects of CaO addition and strain rate on the texture evolution of AZ31 alloy. Materials Science & Engineering A., 744, Pp. 724–732.
- Wang, N., Yang, Q., Li, X., Guan, K., Zhang, J., Yao, C., Zhang, X., Meng, J., Qi, X., 2021. Microstructures and mechanical properties of a Mg-9Gd-3Y-0.6Zn-0.4Zr (wt.%) alloy modified by Y-rich misch metal. Materials Science & Engineering A., 806, Pp. 140609.
- Yan, C., Xin, Y., Chen, X.B., Xu, D., Chu, P.K., Liu, C., Guan, B., Huang, X., and Liu, Q., 2021. Evading strength-corrosion tradeoff in Mg alloys via dense ultrafine twins. Nature communications, 12, Pp. 4616.
- Yuan, W., Panigrahi, S.K., Su, J.Q., and Mishra, R.S., 2011. Influence of grain size and texture on Hall–Petch relationship for a magnesium alloy. Scripta Materialia, 65, Pp. 994–997.
- Zha, M., Ma, X., Jia, H.L., Zhao-Xu Fan, Z.M.H., Yang, Z.Z., Gao, Y.P., Wang, H.Y., 2023. Dynamic precipitation and deformation behaviors of a bimodal-grained WE43 alloy with enhanced mechanical properties. International Journal of Plasticity, 167, Pp. 103682.

